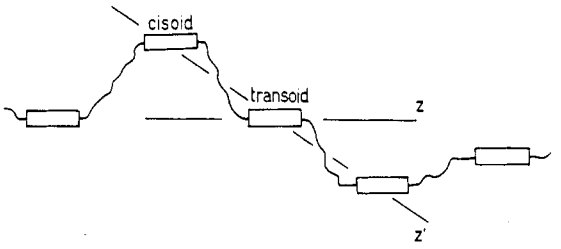

Figure 5. Schematic picture of the situation of a chain in the nematic state. The coexistence of equivalent transoid and cisoid enchainments astride mesogen units gives rise to an average chain axis z substantially parallel to the rigid units. Any z', connecting two subsequent mesogens, can lead, in the case of polymers, to unlikely estimates of this axis.

in case of polymer chains, to unreliable estimates of the average chain axis.

The valence angle at the ether oxygen is now set at 118°, in agreement with crystallographic data on model compounds. The result of these geometrical changes is that of giving rise to a θ_2 angle of ca. 10° between z and z_c. This increases the orientational order parameter of ca. 5% relative to the values obtained in paper 1. A smaller effect, ca. 2%, is predicted on the orientational order parameter obtained from ^{1}H NMR due to the slight tilting of the phenylene rings with respect to the new average chain axis. The new values range from 0.79 to 0.86 as the temperature decreases from 216 °C (the isotropic–nematic transition temperature) to 180 °C. Such effects are small enough to leave all conclusions drawn in paper 1 substantially unchanged.

Concluding Remarks

Decoupling of coformational jumps from chain reorientational motions rests on the different correlation times of these two kinds of motion. This approach allows for a more realistic definition of the average chain axis and for a more reliable valence angle, at the ether oxygen atom *without any modifications of the calculated ^{2}H NMR spectrum* and only small adjustments of the orientational order parameters obtained from ^{2}H and ^{1}H NMR data. This is due to the fact that polymethylene spacers with an even number of chains atoms keep, in the highly extended conformations, the average chain axis z very close to z_c, with an angle θ_2 on the order of a few degrees. From this observation we can immediately devise an interesting extension of the present analysis to the case of spacers with an odd number of chain atoms. In this case, in fact, the highly extended conformers cannot keep the mesogens parallel to each other but rather tilted at ca. 60° [6] so that a much stronger effect from $P_2(\cos\theta_2)$ is expected on the S' factor (see eq 2), giving rise to smaller observed splittings, while conformational mobilities are not expected to depart substantially from the results of calculations already carried out for the even-membered spacer,[6] where three quadrupolar splittings, with different relative magnitudes, are computed as the elongation of the spacer is changed.

Acknowledgment. I thank the Max Planck Society for financial support and am indebted with Prof. H. W. Spiess for very helpful discussions.

Registry No. PDCB-d_{20}, 112220-29-8.

References and Notes

(1) Brückner, S.; Scott, J. C.; Yoon, D. Y.; Griffin, A. C. *Macromolecules* **1985**, *18*, 2709.
(2) Collignon, J.; Sillescu, H.; Spiess, H. W. *Colloid Polym. Sci.* **1981**, *259*, 220.
(3) Geny, F.; Monnerie, L. *J. Polym. Sci., Polym. Phys. Ed.* **1979**, *17*, 147.
(4) Sigaud, G.; Yoon, D. Y.; Griffin, A. C. *Macromolecules* **1983**, *16*, 875.
(5) Hummel, J. P.; Flory, P. J. *Macromolecules* **1980**, *13*, 479.
(6) Yoon, D. Y.; Brückner, S. *Macromolecules* **1985**, *18*, 651.

Affinity of Grain Deformation in Mesomorphic Block Polymers Submitted to Simple Elongation

R. Séguéla and J. Prud'homme*

Laboratoire de Structure et Propriétés de l'État Solide, Université des Sciences et Techniques de Lille, 59655 Villeneuve d'Ascq, France, and Department of Chemistry, University of Montréal, Montréal, Québec, Canada H3C 3V1. *Received August 4, 1987*

ABSTRACT: Small-angle X-ray scattering (SAXS) and strain measurements were performed at various orientations with respect to the stretching direction of a polybutadiene–hydrogenated elastomeric polystyrene–polybutadiene–polystyrene (SBS) block polymer cast under the form of either cylindrical or spherical morphology. The two materials consisted of randomly oriented grains having either an hexagonal packing of polystyrene cylinders or a predominant face-centered-cubic packing of polystyrene spheres. Because both these materials exhibited an isotropic and isochoric macroscopic deformation in agreement with the strain ellipsoid model, they were considered as model systems for applying a general relation proposed for testing the affinity of grain deformation in mesomorphic block polymers. In this relation also based on the strain ellipsoid model, the Bragg spacing strain, d/d_0, for a family of planes with their normal at an angle ω with respect to the stretching direction is given as a function of ω and the longitudinal macroscopic strain, α_x, by the formula $d/d_0 = [\alpha_x^2 \cos^2\omega + (1/\alpha_x)\sin^2\omega]^{1/2}$. Upon stretching, the SAXS patterns of both the cylindrical and the spherical SBS-H systems exhibited elliptical lattice reflections from which were computed Bragg spacing strain d/d_0 values in good agreement with the proposed formula. The tests were limited to an upper draw ratio of 2.3 above which the lattice reflections were either severely truncated or nearly superimposed.

Introduction

Thermoplastic two-phase elastomers consisting of block, graft, or segmented polymers exhibit unique mesomorphic structures and mechanical properties that have stimulated a great deal of applied and theoretical works in the literature.[1] Among these materials, styrene–diene polystyrene–polybutadiene–polystyrene (SBS) and polystyrene–polyisoprene–polystyrene (SIS) three-block polymers have been extensively studied. They are known to yield mesomorphic structures in which, depending upon their composition and their preparation, the cross-linking polystyrene microphase takes the form of spheres, cylinders, or lamellae arranged in regular arrays over large domains of the material. In fact, these domains form

0024-9297/88/2221-0635$01.50/0

grains large enough to yield well-defined X-ray diffraction patterns from which their structure can be characterized. Although some important features concerning the modifications of their mesomorphic structures upon macroscopic deformations such as simple elongation or simple shear have been documented in the literature,[2-10] their deformation mechanisms at the microscopic level is far from being fully understood.

In a previous paper[11] we reported that a polybutadiene hydrogenated SBS polymer (hereafter designated as SBS-H sample) having a polystyrene weight fraction of 0.29 can yield solvent-cast film specimens in which spherical, cylindrical, or lamellar polystyrene microdomains are formed, depending on the solvent used for their preparation. When cast from heptane solution, the SBS-H sample yields specimens with spherical morphology that exhibit nearly reversible stress–strain curves similar to that of unfilled vulcanized rubber. In contrast, cyclohexane yields specimens with cylindrical morphology that show stress softening upon their first extension, while toluene yields specimens with lamellar morphology that exhibit yield and neck propagation. Note that these three solvents are all good solvents for hydrogenated polybutadiene but exhibit marked affinity differences for polystyrene, heptane being a precipitant, cyclohexane a poor solvent, and toluene a good solvent for that polymer.

In a more recent paper[12] we reported a small-angle X-ray scattering (SAXS) study devoted to the deformation behavior of the lamellar SBS-H specimens cast from toluene solutions. The structural changes occurring in the necking process of these specimens consist of a cascade of events involving first a disruption of the polystyrene microphase in the less ordered regions located at the grain boundaries followed by a rotation and a shear of the lamellar grains. The latter process occurs once the direction of the lamellae reaches an orientation close to 20° with respect to the stretching direction. This succession of events was interpreted as the lowest energy path imposed by the mechanical anisotropy of the grains. It was also shown that the deformation of the rubbery chains within the grains was affine with respect to the macroscopic deformation. a similar study was made on the specimens cast from cyclohexane and heptane solutions. Owing to their well-defined morphologies, both these latter types of specimens also provided SAXS data that can be used for an interpretation of their deformation mechanisms at the microscopic level. The present paper describes the most significant results inferred from this study together with considerations related to the interpretation of the SAXS data showing that measurements performed on stretched specimens may contribute to a better characterization of the mesomorphic structures of elastomeric block polymers. Also described is a theoretical relation based on the strain ellipsoid model that can be used for testing affinity of grain deformation in these materials.

Experimental Section

Materials. The polybutadiene hydrogenated SBS block polymer (SBS-H) was a commercial polymer manufactured by Shell Chemical Co. under the name Kraton GX-6500. Its number-average molecular weight was 6.9×10^4 and its polystyrene weight fraction was 0.29. Other characteristics concerning the chemical structure of its midblock and its thermal properties are given in a previous paper.[11] Film specimens of the SBS-H sample were prepared by solvent casting at room temperature from 5% solutions. The solutions were filtered and poured into a rectangular (6 cm × 6 cm) stainless steel frame partially immersed into mercury. The casting unit was set up into a laboratory dessicator in which an appropriate and gradual reduction of pressure was applied in order to slowly evaporate the solvent for a period of 3–4 days. The film specimens about 0.7 mm thick were subsequently dried for a week under high vacuum. The specimens with cylindrical morphology were obtained from cyclohexane solutions while those with spherical morphology were obtained from heptane solutions. Both solvents were reagent grade materials. Test pieces for SAXS and strain measurements were cut into rectangular strips about 3 cm long and 0.5 cm wide. They were stretched and held to appropriate draw ratios by means of a homemade screw-controlled extension holder fitted out with flat jaws.

Small-Angle X-ray Scattering and Strain Measurements. The small-angle X-ray scattering patterns were recorded on photographic films with a Model 2202 Rigaku-Denki goniometer provided with a two-pinhole collimator. Ni-filtered Cu Kα radiation (λ = 0.154 nm) was generated by a Philips tube operated at 40 kV and 20 mA. The second pinhole, specimen, and photographic film were placed at 300, 320, and 630 mm from the first pinhole, respectively. For each draw ratio, a series of three patterns were recorded with increasing exposure time. For the first pattern of the series the collimator assembly consisted of 0.3- and 0.2-mm pinholes while for the other patterns it consisted of wider 0.5- and 0.3-mm pinholes. The X-ray beam impingement was centered into a circular ink mark of about 1-mm diameter drawn on the plane of the unstretched specimen. The actual longitudinal strain, α_x, along the stretching direction was determined by measuring the deformation of this mark with a microscope before and after each SAXS recording. Strains α_ω at various angles ω with respect to the stretching direction were also measured by the same technique. The intensity profile along the equator in some of the SAXS patterns were recorded from the photographic films with a Joyce-Loebl microdensitometer.

Results and Discussion

1. SBS-H Specimens with Cylindrical Polystyrene Microdomains. SAXS patterns recorded for different longitudinal strains, α_x, ranging from 1 to 4.45 are presented on Figure 1. For each strain, three patterns are shown with increasing exposure time from the left to the right. Their whole scattering consists of three diffraction orders that are gathered in schematic diagrams depicted on the last column of Figure 1. As shown in a previous paper devoted to the structure characterization of the SBS-H specimens,[11] the first and second diffraction orders for the unstretched material correspond to lattice reflections issued from the {10} and {11} planes in ordered grains consisting of hexagonally packed parallel cylinders. Initially, these grains are randomly oriented as indicated by the circular patterns observed for $\alpha_x = 1$. Their unit-cell dimension is a = 32.7 nm and the radius of the polystyrene cylinders is R = 8.6 nm.[11] The third diffraction order is due to particle scattering modulated by ill-defined reflections issued from the hexagonal lattice. Indeed, as shown in Figure 2, this scattering maximum coincides perfectly with the second maximum of the single particle scattering envelope predicted for an infinite solid cylinder of radius R = 8.6 nm, according to the following relation:[13]

$$I \propto F^2(hR) = (2J_1(hR)/hR)^2 \quad (1)$$

where $F(hR)$ is the so-called particle factor, J_1 is the Bessel function of the first order, and $h = (4\pi/\lambda) \sin \theta$. The scattering angle is 2θ and λ = 0.154 nm.

It may be seen in Figure 1 that, with increasing longitudinal strain, α_x, the initially circular {10} and {11} lattice reflections become elliptic with quadrant maxima that gradually transform into four-point diagrams. At first glance, this suggests an elongation of the grains along the stretching direction with a concomitant orientation of the cylinders in preferential directions inclined with an axial symmetry with respect to the stretching direction. However, another phenomenon contributes to the buildup of the four-point diagrams. Indeed, as the lattice reflections become elliptic, their prolate ends fall into the angular

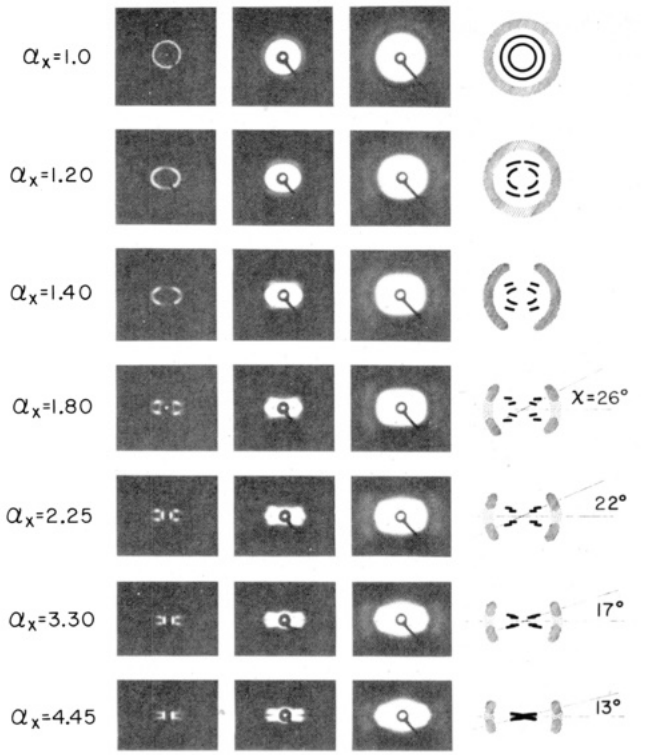

Figure 1. SAXS patterns recorded for different longitudinal strains, α_x, applied to the SBS-H specimens with cylindrical morphology. The stretching direction is vertical.

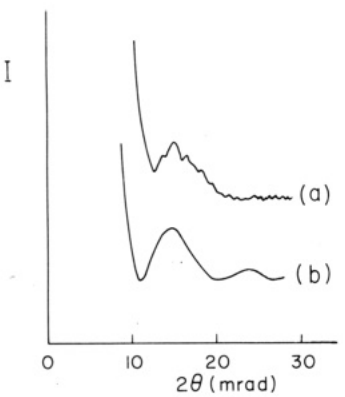

Figure 2. Intensity profile recorded along the equator in the region of the particle scattering ring observed for the SBS-H specimens with cylindrical morphology (curve a) compared to the theoretical scattering envelope computed according to eq 1 for an infinite solid cylinder of radius R = 8.6 nm (curve b).

region where the particle factor $F(hR)$ exhibits a first extinction in its damped periodic profile (see Figure 2). Since the intensity of the lattice reflections is modulated by the quantity $F^2(hR)$,[13] their integrity is not preserved over the angular range where $F(hR)$ becomes infinitely small. This effect can be clearly identified in the patterns recorded at α_x = 1.20 in Figure 1 in which the larger {11} reflection is severely truncated at its prolate ends along the equator, though the smaller {10} reflection is only slightly attenuated in this region. Note that such a casual effect related to the particle factor has been previously identified by Hadziioannou et al.[9] on SAXS patterns recorded for a stretched SIS specimen perfectly oriented under the form of a hexagonal single crystal, the stretching direction being perpendicular to the cylinder direction. Because of this effect, it is not possible to perform a quantitative analysis of the lattice deformation of the grains in the present cylindrical specimens similar to that we reported for the

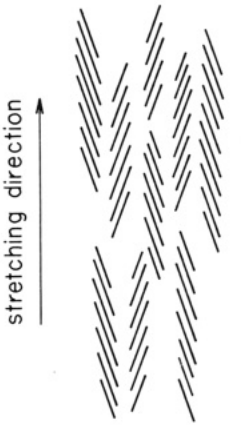

Figure 3. Schematic illustration of the fiberlike structure that would account for the four-point patterns observed in Figure 1 for strain values greater than 2.3. This structure involves elongated grains having their cylinders slightly inclined at an angle χ with an axial symmetry with respect to the stretching direction.

SBS-H lamellar specimens.[12]

Nevertheless, as shown on the schematic diagrams in Figure 1, quantitative information concerning the cylinder orientation can be obtained from the third diffraction order assigned to the second maximum of the particle scattering envelope. First, it may be seen that a gradual extinction of these scattering occurs on the meridian with increasing longitutinal strain in the range from 1 to 1.40. Note that a similar extinction is also observed for the first and second diffraction orders issued from the lattice. This indicates that the grains with their cylinders perpendicular to the stretching direction are the first to undergo rotation or disruption in the material. Second, it may be seen that upon further elongation a quadrant diagram develops for the third-order diffraction, though the intensity of the latter does not fade out completely on the equator. This quadrant diagram makes it possible to estimate the average orientation angle χ of the cylinders with respect to the stretching direction. As shown on the schematic diagrams, χ decreases from 26° to 13° with increasing strain in the range from 1.80 to 4.45.

The progressive transformation of the two initially circular {10} and {11} lattice reflections into the form of two distinct four-point diagrams which remain resolved up to a strain value close to 2.3 is a clear indication that the polystyrene cylinders keep their two-dimensional organization up to an advanced stage of the macroscopic deformation. For strains above this latter value, the two reflections merge into a single four-point diagram with elongated lobes nearly perpendicular to the stretching direction. This latter pattern suggests a fiberlike structure similar to that pictured in Figure 3, in which the grains are elongated along the stretching direction with their parallel cylinders still slightly inclined (χ = 13°) with respect to this direction. At this stage of the deformation, the structure of the present material is very similar to that previously inferred for the lamellar SBS-H material at the highest local strain (α_x = 2.3) measured in its neck region.[12] Also, like the lamellar material, the present material could recover its initial isotropic structure when relaxed for a few minutes after a stretching cycle to α_x = 4. This has been evidenced by the recovery for the retracted specimens of circular patterns identical with those measured prior to their stretching. Nevertheless, while the circular patterns of the lamellar material exhibited extinction on the me-

ridian indicating an irreversible disruption of its grains having their lamellae perpendicular to the stretching direction, those of the present material exhibited uniform intensity for any asimuth including the meridian. This suggests that the disruption of the rigid microphase at the origin of the stress softening effect observed upon the first stretching of the cylindrical material[11] is selectively located within the ill-organized regions at the grain boundaries where the rigid microphase does not participate to microcomposite entities having well-defined cooperative responses such as change in orientation and shear when submitted to external forces.

In the case of the SBS-H lamellar specimens,[12] a rotation of the grains occurred from the very beginning of the neck deformation and was about completed for a local strain α_x close to 1.2. At this stage, the lamellae were oriented at an angle χ close to 22° with respect to the stretching direction. Upon further local elongation in the neck region, a gradual shear of the rigid lamellae contributed to orient the grains parallel to the stretching direction without a significant change of the lamella orientation (χ = 17° for α_x = 2.30).[12] This behavior can be rationalized by considering that the lamellar grains are more liable to deform by simple shear than by simple elongation because the latter deformation is hindered by the higher energy required for the concomitant lateral contraction of the rubbery lamellae. Indeed, such a contraction would involve larger stresses applied to the individual rubbery chains anchored to the rigid lamellae than those resulting from the shear process. Obviously, the grains with their lamellae perpendicular to the stretching direction were not able to deform by simple shear. They were rather submitted to a simple elongation which early gave rise to an irreversible disruption promoted by the latteral contraction of the rubbery lamellae. The situation is not the same for the present SBS-H specimens because a great part of the stress due to the lateral contraction of the rubbery microphase can be relaxed through an appropriate lateral displacement of the hard cylinders. Therefore, contrary to the sheared lamellar grains which retained their lamellar packing all along the neck deformation up to α_x values as great as 2.3, a significant distorsion of the hexagonal packing occurs from the beginning of the deformation of the present material as evidenced by a significant departure of the d_{10}/d_{11} spacing ratio from the value $3^{1/2}$ expected for such a packing.[11] Indeed, when directly measured on the quadrant maxima in Figure 1, the d_{10}/d_{11} ratio decreases from 1.69 to 1.49 with increasing α_x from 1 to 1.80.

A last remark concerns the quadrant maxima observed for the third diffraction order in Figure 1, that is, the diffraction order associated with the second maximum of the particle scattering factor $F(hR)$. As pointed out previously, the intensity of this scattering does not vanish completely on the equator. As will be shown shortly, this particularity can be predicted theoretically for the scattering by a large number of infinite solid cylinders uniformly distributed at a given inclination with respect to the stretching direction and thus does not necessarily mean that some of the cylinders are oriented parallel to the stretching direction. Figure 4 depicts the direct and the reciprocal images of a cylinder oriented at an angle χ with respect to the x-axis previously defined as the stretching direction. The direction of the incident beam is along the z-axis. The polar angles φ and μ define the projection of the cylinder on the yz and the xy planes, respectively. From the geometry of the direct image it may be seen that the relation between the angular variables is

$$\tan \mu = \tan \chi \sin \varphi \qquad (2)$$

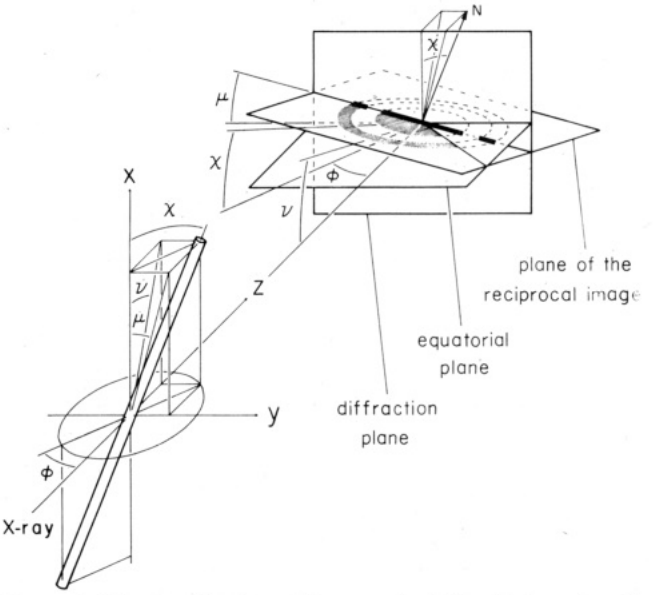

Figure 4. Direct and reciprocal images of a solid cylinder oriented at an angle χ with respect to the stretching direction (x-axis). The diffraction pattern is shown by the thick line at the intersection of the reciprocal image and the diffraction plane. See the text for the other details.

In Figure 4, the first and the second orders of the reciprocal image are respectively represented by a flat disk and a concentric ring whose common normal N is parallel to the cylinder axis. The scattering pattern is shown by the thick line at the intersection of the reciprocal image and the diffraction plane. Its radial intensity varies according to eq 1 and its orientation with respect to the equator (y-axis) is defined by the polar angle μ. According to eq 2, it may be shown that for a given inclination χ of the cylinder, the rotation of the latter about the x-axis produces a periodic change in the orientation of the linear pattern in which μ oscillates from the value $-\chi$ to the value $+\chi$. However, in the case of a large number of cylinders having the same inclination χ and being uniformly distributed over all orientations in the range $0 \leq \varphi < 2\pi$, the scattering intensity at 2θ is not uniformly distributed over the range $-\chi \leq \mu \leq +\chi$. Indeed, the fraction, $f(\mu,\chi)$, of the cylinders giving rise to scattering along the azimuth μ is given by the relation

$$f(\mu,\chi) = A/[[1 - (\tan \mu/\tan \chi)^2]^{1/2} \tan \chi \cos^2 \mu] \qquad (3)$$

in which A is a normalization constant. Equation 3 can be derived from the cumulative distribution of φ

$$F(\varphi) = \varphi/2\pi \qquad (4)$$

by the differentiation of the latter with respect to μ after an appropriate change of variables according to eq 2.

Figure 5 shows a plot of $f(\mu,\chi)$ as a function of μ for the value χ = 26°. From this plot it may be inferred that, though the scattering intensity should exhibit a sharp maximum at $\mu = \chi$, it should not vanish at μ = 0, on the equator of the diffraction plane. Obviously, any fluctuation of the cylinder inlination with respect to the preferential inclination χ shall contribute to flatten the scattering peak at $\mu = \chi$. Thus, the features of the quadrant scattering observed in Figure 1 are qualitatively in agreement with the present model.

Figure 6 shows the variation of the macroscopic strain, α_ω, measured in the plane of the film specimens for different orientations in the range $0° \leq \omega \leq 90°$ with respect to the stretching direction. Data points are plotted for four values of the longitudinal strain (α_x = 1.20, 1.40, 1.80, and

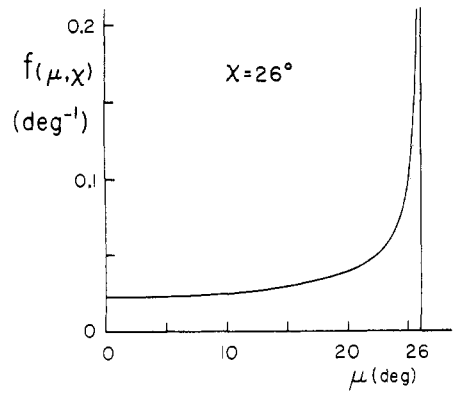

Figure 5. Distribution profile, $f(\mu,\chi)$, for randomly oriented cylinders inclined at an angle χ with respect to the stretching direction that have the correct orientation for giving rise to scattering along the azimuth μ on the diffraction plane. Plotted as a function of μ according to eq 3 for the particular case χ = 26°.

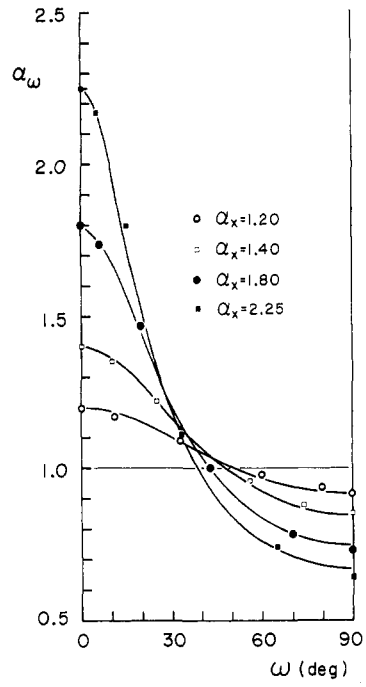

Figure 6. Macroscopic strains, α_ω, measured in the plane of the SBS-H film specimens with cylindrical morphology for various angles ω with respect to the stretching direction. Data points plotted as a function of ω for different values of the longitudinal strain, α_x, together with the corresponding theoretical curves computed according to eq 5 for the strain ellipsoid model.

2.25). Also shown in Figure 6 are corresponding theoretical curves calculated according to the following relation derived from the well-known strain ellipsoid model for a constant-volume uniaxial tensile deformation:[12]

$$\alpha_\omega = [\alpha_x^2/(\alpha_x^3 \sin^2 \omega + \cos^2 \omega)]^{1/2} \quad (5)$$

It may be seen that the fit provided by eq 5 is excellent for the four values of α_x, indicating that the macroscopic deformation is both isotropic with respect to the stretching direction and isochoric.

From the same model, it is also possible to derive a law of affinity for the microscopic deformation. In order to apply such a law in terms of the diffraction data observed for various values of the longitudinal strain, α_x, one must first derive the change in the spacing d between two consecutive diffracting planes produced by a local deformation affine with respect to the macroscopic deformation. Owing to the symmetry of revolution of the overall transformation

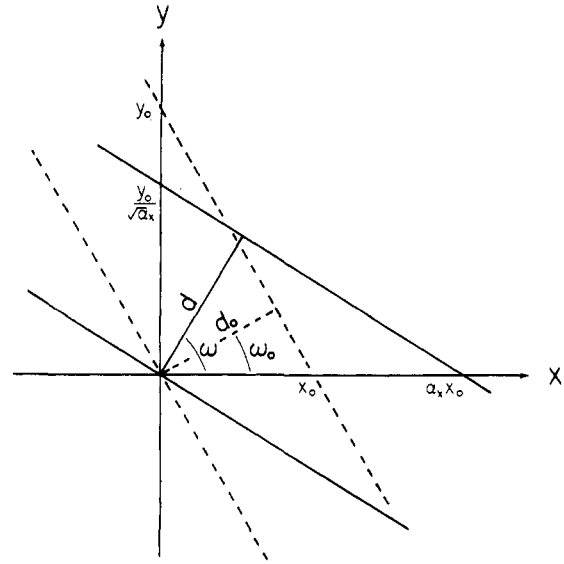

Figure 7. Two-dimensional analysis for the change in the spacing d between two consecutive diffracting planes in grains undergoing an affine deformation with respect to the strain ellipsoid model. Upon stretching along the x-axis, the normal to the planes rotates from an angle ω_0 to an angle ω and the spacing between planes changes from d_0 to d. The variation of d/d_0 as a function of both ω and α_x is given by eq 6.

with respect to the stretching direction, the problem can be reduced to the two-dimensional analysis pictured in Figure 7. Upon stretching, the normal to the planes rotates from an angle ω_0 to an angle ω with respect to the x-axis and the spacing changes from d_0 to d. The rotation is caused by the difference between the strain along the x-axis, α_x, and that along the y-axis, $\alpha_y = 1/\alpha_x^{1/2}$, as imposed by the strain ellipsoid model. Geometric analysis yields the following relation for the variation of d/d_0 as a function of both α_x and ω

$$d/d_0 = [\alpha_x^2 \cos^2 \omega + (1/\alpha_x) \sin^2 \omega]^{1/2} \quad (6)$$

Note that the ratio d/d_0 corresponds to the Bragg spacing strain for any family of planes having their normal oriented at an angle ω with respect to the stretching direction. Figure 8 shows the variation of this ratio as a function of ω for the first-order Bragg spacings measured at various orientations in the range $0° \leq \omega \leq 90°$ on the SAXS patterns recorded for the same values of the macroscopic strain, α_x, as in the preceding analysis. Also shown in Figure 8 are the corresponding theoretical curves computed according to eq 6. It may be seen that these curves provide an excellent fit to the data points measured at α_x = 1.20 and good fits to the data points measured in the range $1.40 \leq \alpha_x \leq 2.25$. Note that the latter data points are restricted to a decreasing range of ω with increasing α_x because of the quadrant nature of the patterns for strain values above 1.2.

2. SBS-H Specimens with Spherical Polystyrene Microdomains. Structure and properties of SIS and SBS block polymers with spherical morphology are well documented in the literature.[1] Nevertheless, the characterization by SAXS of the periodic arrangement of their spheres in terms of any one of the three classical cubic lattices or the close-packed hexagonal lattice has often been problematic.[14-18] As for the lamellar or the cylindrical systems, the approach used for identifying the actual structure by means of SAXS powder patterns is to compare the Bragg spacing ratios d_1/d_n (n = 1, 2, 3, ..., p) of the p observed reflections with the corresponding theoretical ratios computed from the appropriate classical formulas.[19] The discriminating power of this approach can

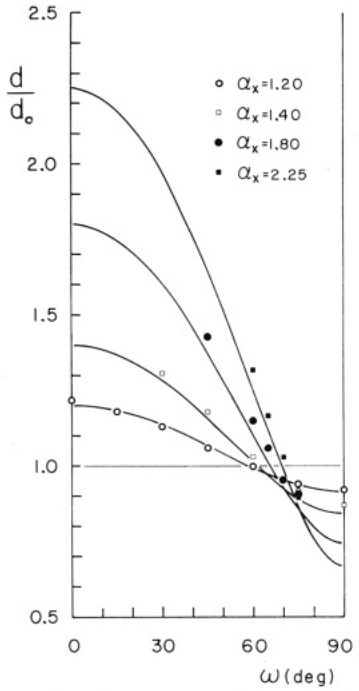

Figure 8. First-order Bragg spacing strains, d/d_0, measured on the SAXS patterns of the SBS-H specimens with cylindrical morphology for various angles ω with respect to the meridian (stretching direction). Data points plotted as a function of ω for the same values of the macroscopic strain, α_x, as in Figure 6, together with the corresponding theoretical curves computed according to eq 6 for an affine deformation.

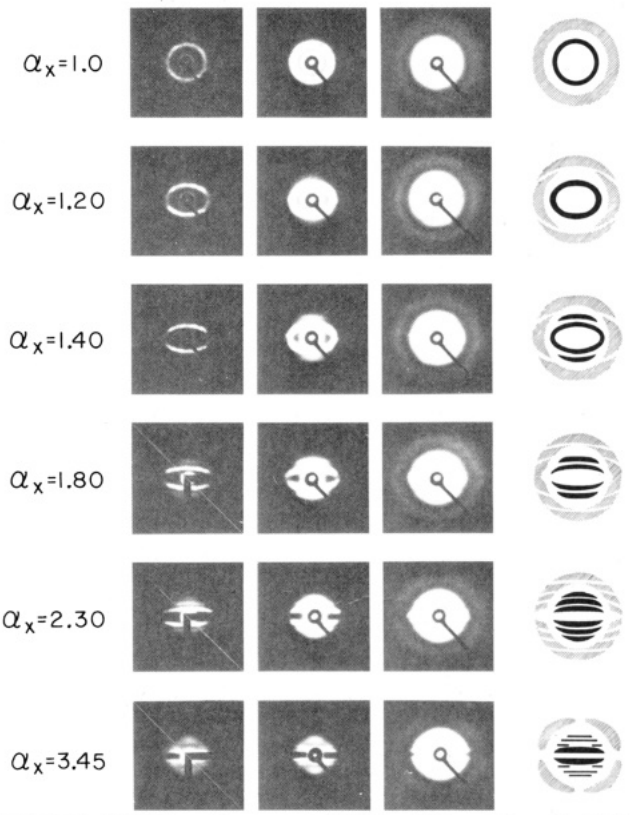

Figure 9. SAXS patterns recorded for different longitudinal strains, α_x, applied to the SBS-H specimens with spherical morphology. The stretching direction is vertical.

be visualized by considering the following series of d_1/d_n ratios characterizing the first six reflections expected for the four lattices mentioned above: 1.00, 1.41, 1.73, 2.00, 2.24, 2.45, for simple cubic or body-centered cubic; 1.00, 1.15, 1.63, 1.91, 2.00, 2.31, for face-centered cubic; 1.00, 1.06, 1.13, 1.46, 1.73, 1.88, for close-packed hexagonal.

For block polymers with spherical morphology, unambiguous fitting of the diffraction data by one of these characteristic ratio series has been possible in a few cases only,[20-23] among which are recent studies performed by small-angle neutron scattering (SANS) on SB and SI two-block polymers.[22,23] From these studies, it appears that either of the two characteristic ratio series expected for the various cubic lattices could be observed depending upon the nature of the block polymer, its composition, and the specimen preparation. In most of the other reported studies, packing assignments were made difficult because of systematic extinctions apparently due to casual effects associated with the particle factor. Also observed in some cases were important departures between the experimental and theoretical values of some of the characteristic ratios. For instance, in the case of solvent-cast SBS polymers, the literature reports a study in which the observed d_1/d_n ratios of 1.00, 1.47, and 2.35 were assigned to a simple cubic lattice[14] and another study in which the observed ratios of 1.00, 1.63, and 2.62 were tentatively assigned to a face-centered cubic lattice.[15]

There is no reason why structured grains consisting of a large number of spheres should not be present in these latter materials as in the lamellar and cylindrical materials. Moreover, there are good reasons for expecting a close-packed arrangement for the spheres, at least for materials prepared by solvent casting under equilibrium conditions. Indeed, by assuming that the morphology of a solvent-cast ABA block polymer is governed by the micellar arrangement of the swollen system just before its solidification, and that this geometry depends upon the relative volumes of the swollen A and B phases, it is easy to visualize that the microdomains forming the dispersed phase are enveloped by a more or less uniform shell of the incompatible blocks anchored to them. This shell produces a repulsive force between the nearest-neighbor microdomains that should keep them at an equal distance from each other. This statement previously formulated by Hoffmann et al.[24] has been reinforced by Meier[25] who showed that the probability for a B chain to be anchored to microdomains A being next-nearest neighbors for each other is negligible. Note that among the cubic lattices mentioned above, the face-centered lattice is also a close-packed arrangement. With respect to the nearest-neighbor sphere interactions, the latter is stricly equivalent to the close-packed hexagonal lattice. Surprisingly, the literature data concerning SAXS studies as well as more recent SANS studies[22,23] made on solvent-cast block polymers do not confirm the generality of a close-packing arrangement for the spherical system. This, together with the difficulty for observing unambiguous lattice reflections, has led many authors to the conclusion that the spherical system is generally less ordered than the lamellar and the cylindrical systems.

In the case of the present SBS-H material with spherical morphology, a first evidence for the presence of structured grains may be observed directly on the low-exposure SAXS pattern of the unstretched specimen (upper left pattern in Figure 9) that exhibits distinctive diffraction spots unevenly distributed all over its single diffraction ring. Furthermore, the radial position of some of these spots appears to be eccentric with respect to the middle part of the ring, suggesting the coexistence of two kinds of grains in the present material.

As depicted on the schematic diagrams at the right of the patterns in Figure 9, the whole scattering recorded for different longitudinal strains in the range $1 \leq \alpha_x \leq 3.45$ consists of lattice reflections surrounded by a larger ring

issued from particle scattering. For the stretched specimens, the latter remains circular but appears to be slightly modulated by elliptical intereferences. On the other hand, as for the SBS-H cylindrical material, upon stretching, the initially circular single lattice reflection becomes elliptical and its prolate ends are progressively truncated on the equator when they fall into the scattering angle region where the particle scattering envelope exhibits its first extinction. Inversely, because of the decrease in the reciprocal Bragg spacings along the stretching direction, a second lattice reflection appears in the meredian region for $\alpha_x > 1.4$, then a third one for $\alpha_x < 1.8$, followed by a fourth one for $\alpha_x < 2.3$. These latter reflections are enhanced with increasing strain because they are progressively displaced toward the origin into the scattering angle region where the particle scattering envelope exhibits its first maximum.

Figure 10 shows a microdensitometric curves recorded along the equator in the region of the particle scattering ring observed for the unstretched specimen. This curve exhibits a second scattering peak that was too weak to be reproduced on the photographs of Figure 9. Also shown in Figure 10 is a theoretical scattering curve computed from the particle factor for a single solid sphere of radius R according to the relation[26]

$$I \sim F^2(hR) = [3(\sin hR - hR \cos hR)/(hR)^3]^2 \quad (7)$$

As it may be seen, an excellent fit of the two scattering peaks can be obtained by adjusting the value of R to 9.7 nm in eq 7. This fitting may be considered as a characterization of the radius of the polystyrene spheres in the present SBS-H material.

The Bragg spacings corresponding to the first-order indexed reflection for each of the lattices mentioned before are given as a function of the radius R and the volume fraction ϕ_s of the spheres one can derive from the geometrical properties of these lattices by the following relations:

$$\text{simple cubic:} \quad d_{100} = (4\pi/3\phi_s)^{1/3}R \quad (8)$$

$$\text{body-centered cubic:} \quad d_{110} = 2^{1/2}(\pi/3\phi_s)^{1/3}R \quad (9)$$

$$\text{face-centered cubic:} \quad d_{111} = (2/3^{1/2})(2\pi/3\phi_s)^{1/3}R \quad (10)$$

$$\text{close-packed hexagonal:} \quad d_{100} = (3/2)^{1/6}(\pi/\phi_s)^{1/3}R \quad (11)$$

By using the quantity $R = 9.7$ nm obtained from the preceding analysis of the particle scattering envelope and the volume fraction $\phi_s = 0.25$ previously characterized for the present SBS-H sample,[11] one can compute the following values for the Bragg spacing and the scattering angle 2θ of the first-order lattice reflection predicted for each of the four lattices: simple cubic, $d_{100} = 24.8$ nm, $2\theta = 6.2$ mrad; body-centered cubic, $d_{110} = 22.1$ nm, $2\theta = 7.0$ mrad; face-centered cubic, $d_{111} = 22.8$ nm, $2\theta = 6.8$ mrad; close-packed hexagonal, $d_{100} = 24.1$ nm, $2\theta = 6.4$ mrad.

The actual values of the scattering angle 2θ observed for the first-order diffraction ring in Figure 9 is close to 6.6 mrad. That for the eccentric spots on the latter is close to 6.9 mrad. Though there is a good agreement between these values and the rather narrow range of 2θ expected for the four plausible lattices, the present comparison based on the values of R and ϕ_s is not accurate enough for an assignment among the latter.

The next step is to consider the Bragg spacing ratios d_1/d_n of the various lattice reflections appearing on the patterns recorded for the stretched specimens. These ratios were evaluated for the Bragg spacings measured on the meridian for each of the observed reflections. As shown in Table I, the value of d_1/d_2 slightly increases from 1.62 to 1.73 with increasing strain from 1.40 to 3.45. Similarly, the value of d_1/d_3 increases from 2.30 to 2.6 with increasing strain from 2.30 to 3.45. Finally, the single value of d_1/d_4 measured for $\alpha_x = 3.45$ is close to 3.3. The data for d_1/d_2 and d_1/d_3 can be linearly extrapolated to the values 1.60 and 1.96, respectively, at $\alpha_x = 1$. Among the four d_1/d_n ratio series previously quoted, that for a face-centered cubic lattice (1.00, 1.15, 1.63, 1.91, 2.00, 2.31) would give the best fit to the present data. Indeed, if one considers that the second member of this series is rather close to unity, it may be assumed that the first two orders were not resolved on the present SAXS patterns. Because of that, the apparent d_1/d_2 ratio extrapolated to 1.60 would correspond to the real ratio d_1/d_3 underestimated by about 2% with respect to its expected value of 1.63. On the other hand, the apparent d_1/d_3 ratio extrapolated to 1.96 would roughly correspond to the real ratio d_1/d_4 overestimated by about 3% with respect to its expected value of 1.91. Note that the latter extrapolation was made with only two data points that were rather distant from the origin. The increase of both the apparent ratios d_1/d_2 and d_1/d_3 with increasing strain as well as the large magnitude of the apparent d_1/d_4 ratio measured for $\alpha_x = 3.45$ indicate that, as for the cylindrical material, an important distorsion of the lattice occurs from the very beginning of the macroscopic deformation.

Finally, concerning the eccentric diffraction spots observed on the first-order ring, the fact that their scattering angle 2θ is slightly greater than that of the main reflection

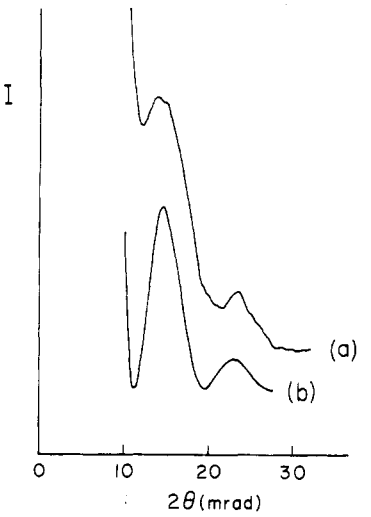

Figure 10. Intensity profile recorded along the equator in the region of the particle scattering ring observed for the SBS-H specimens with spherical morphology (curve a) compared to the theoretical scattering envelope computed according to eq 7 for a solid sphere of radius $R = 9.7$ nm (curve b). The experimental curve shows a second scattering peak not reproduced in the photographic patterns of Figure 9.

Table I
First-Order Bragg Spacings, d_1, and Bragg Spacing Ratios d_1/d_n of the First-Order to the Higher Order Lattice Reflections Measured on the Meridian for Various Longitudinal Strains, α_x, Applied to the SBS-H Specimens with Spherical Morphology

α_x	d_1, nm	d_1/d_2	d_1/d_3	d_1/d_4
1	23.3			
1.20	29.2			
1.40	33.3	1.62		
1.80	42.8	1.64		
2.30	52.4	1.67	2.30	
3.45	80	1.73	2.6	3.3

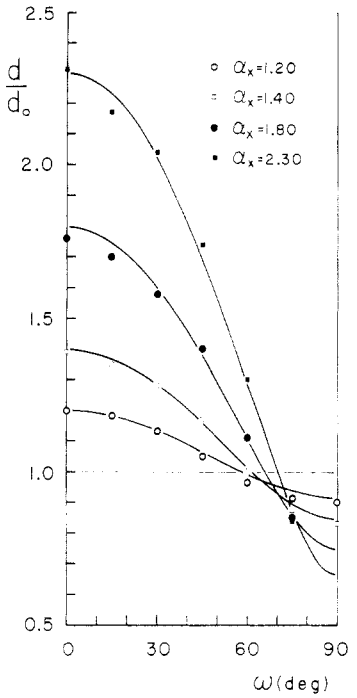

Figure 11. First-order Bragg spacing strains, d/d_0, measured on the SAXS patterns of the SBS-H specimens with spherical morphology for various angles ω with respect to the meridian (stretching direction). Data points plotted as a function of ω for different values of the macroscopic strain, α_x, together with the corresponding theoretical curves computed according to eq 6 for an affine deformation.

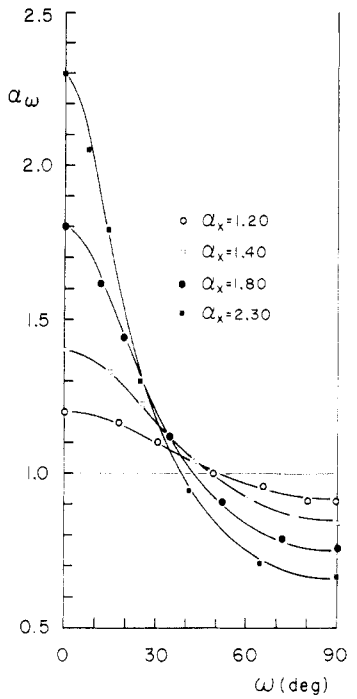

Figure 12. Macroscopic strains, α_ω, measured in the plane of the SBS-H film specimens with spherical morphology for various angles ω with respect to the stretching direction. Data points plotted as a function of ω for the same values of the longitudinal strain, α_x, as in Figure 11, together with the corresponding theoretical curves computed according to eq 5 for the strain ellipsoid model.

assigned to a face-centered-cubic lattice suggests that they are issued from a body-centered-cubic lattice, the only one among the plausible lattices for which a greater scattering angle is expected on the basis of the preceding predictions.

In spite of the apparent lattice distorsion occurring upon stretching, the Bragg spacings measured on the meridian for the first-order lattice reflection appears to be directly proportional to α_x for all strain values including the maximum value of 3.45. This indicates that the change produced in the distance between the {111} diffraction planes of the proposed face-centered-cubic structure is affine for the grains having these planes perpendicular to the stretching direction. In fact, such an affine behavior is also observed for any other orientation of the grains in the material. Indeed, as shown in Figure 11 for different values of the macroscopic strain in the range $1.2 \leqslant \alpha_x \leqslant 2.3$, the variation of the first-order Bragg spacing strain, d/d_0, measured at various angles ω with respect to the stretching direction exhibits an excellent agreement with the theoretical curves predicted for an affine deformation according to eq 6 derived in the preceding section. This latter test for affinity is based upon the strain ellipsoid model which, as shown in Figure 12, also applies to the macroscopic deformation of the present material.

The good fit observed in Figure 11 also confirms that the first diffraction order recorded for the present material is a genuine lattice reflection rather than a scattering peak associated with the periodicity of the nearest-neighbor distance between the spheres. Note that the latter interpretation has often been postulated in previous studies on block polymers with spherical morphology.[14,16] If it were such, the ratios d/d_0 would rather conform to α_ω according to eq 5. The latter describes the relative change of the distance between two points in the material instead of the distance between two diffracting planes. By comparing the d/d_0 data points in Figure 11 with the α_ω theoretical curves in Figure 12, it may be seen that, though these two quantities are (and should be) the same for the directions parallel ($\omega = 0°$) and perpendicular ($\omega = 90°$) to the stretching direction, they differ markedly for any other direction in the range $0° < \omega < 90°$.

Conclusion

In the present study, a general relation for testing affinity of grain deformation in mesomorphic block polymers has been derived from the strain ellipsoid model. In this relation, the change in the distance between consecutive diffracting planes with their normal at an angle ω with respect to the stretching direction is given as a function of ω and the longitudinal macroscopic strain, α_x. By applying this relation to the first-order SAXS lattice reflections recorded for the present cylindrical and spherical SBS-H systems, it has been shown that the deformation of their diffracting grains was affine with respect to the macroscopic deformation. This affine behavior was observed up to a macroscopic strain of 2.3, for which the first-order lattice reflection was still measurable over an acceptable range of ω. Also, by independent measurements it has been confirmed that the strain ellipsoid model provided an excellent fit to the macroscopic deformation of both these materials.

In a previous study,[12] such an affine behavior was also observed for the lamellar SBS-H system. However, in that latter case, the present test for affinity would have been considerably less accurate because the lattice reflections were limited to a narrow range of ω for which, unfortunately, the microscopic strain d/d_0 for the distance between the diffracting planes remained close to unity. Indeed, in the early stage of the deformation of the lamellar material, namely, for a macroscopic strain as low as 1.4, the lamellae were about completely oriented at an angle $\chi = 22°$ with respect to the stretching direction as evidenced by four-point diagrams on the SAXS patterns. This restricted the investigation for affinity to a single

angle $\omega = 90° - \chi$ that slightly increased from 68° to 73° with increasing strain up to 2.3. Inspection of the theoretical curves in either Figure 8 or Figure 11 shows that the microscopic strain d/d_0 expected for an affine behavior in this particular range of ω lies in the range 0.96–0.92. In fact, these latter values of d/d_0 coincide perfectly with the experimental data reported in the previous study.[12] Because of that feature, a different and more accurate test for affinity was derived in terms of three variables including the long-axis direction of the grains in addition to the lamella direction and their spacing strain d/d_0. The long-axis direction of the grains could be measured directly on the SAXS patterns as the orientation of the lobes with respect to the equator in the four-point diagrams.[12] Obviously, this approach cannot be used for the present systems.

In the case of the lamellar system, both the microscopic and the macroscopic deformations were investigated in the neck region where the most important part of the strain occurred upon the first elongation of the specimens.[12] For the present systems, no necking was observed upon their first elongation.[11] On the contrary, the spherical system exhibited a nearly reversible extension cycle up to a strain value as large as 4, while in the same range of strain, the cylindrical system exhibited stress softening but no permanent set when retracted. For the three systems, the conformity of their macroscopic strain in any direction in the plane of the film specimens with that predicted by the strain ellipsoid model indicates a Poisson ratio value close to 0.5 which in turn suggests that the overall deformation mainly resulted from the rubbery microphase with at best a minute amount of ductile deformation of the glassy microdomains. A ductile deformation of the polystyrene microphase occurred for the lamellar and the cylindrical systems only. It was evidenced by neck formation for the former system and by stress softening for the latter system.

The three SBS-H systems could recover their initial SAXS powder patterns when relaxed for a few minutes at room temperature after an extension cycle up to a strain value of 4. However, on the patterns of the relaxed specimens, the meridian diffraction was faded out for the lamellar system,[12] albeit it was not even attenuated for the other two systems. This difference results from the impossibility for the lamellar grains to extensively deform by simple elongation without a concomitant distorsion of the glassy lamellae resulting from the contraction of the rubbery lamellae. Since the lamellar grains having their lamella surfaces perpendicular to the stretching direction cannot deform by either shear or rotation, they undergo local stresses large enough for causing an irreversible disruption of their glassy lamellae. In the case of the cylindrical and spherical systems, the local stresses resulting from the contraction of the rubbery matrix can be relaxed through appropriate displacements of the cylinders or spheres. This produces a distorsion of the grain lattices but without a significant distorsion or disruption of the glassy microdomains. On the other hand, it is likely that the disruption processes accounting for the greatest part of the yield observed for the lamellar system, and also for the stress softening observed for the cylindrical system, occur at the grain boundaries. Unfortunately, SAXS study cannot provide any direct information concerning the nature of these latter disruption processes.

Finally, it has been shown in the present study that SAXS measurements made on stretched elastomeric block polymers may contribute to a better characterization of their mesomorphic structure in the unstretched state. This has been the case for the present SBS-H spherical system for which only the first-order lattice reflection was observed on the SAXS patterns of the unstretched specimen. The observation of a single lattice reflection resulted from a casual effect associated with the volume fraction of the present spherical domains. Indeed, the radius of the polystyrene spheres was such that the scattering factor for a single sphere, $F(hR)$, exhibited its first extinction in the scattering angle region where the next diffraction orders were expected to occur. However, owing to the change in the Bragg spacings produced by stretching the specimens, it has been possible to observe three additional lattice reflections in the meridian zone of the SAXS patterns with increasing macroscopic strain in the range from 1.4 to 3.5. This occurred because, upon stretching, the meridian lattice reflections were displaced toward the origin in the scattering angle region where the particle scattering factor exhibited its first maximum. The Bragg spacings of two of these additional reflections could be extrapolated to unitary strain making it possible to assign a predominant face-centered-cubic packing to the diffracting grains.

Acknowledgment. This work was supported by Natural Sciences and Engineering Research Council of Canada and the Quebec Ministry of Education.

References and Notes

(1) Noshay, A.; McGrath, J. E. *Block Copolymers, Overview and Critical Survey*; Academic: New York, 1977; Chapter 6.
(2) Beecher, J. F.; Marker, L.; Bradford, R. D.; Aggarwal, S. L. *J. Polym. Sci., Part C* **1969**, *26*, 117.
(3) Inoue, T.; Moritani, M.; Hashimoto, T.; Kawai, H. *Macromolecules* **1971**, *4*, 500.
(4) Pedemonte, E.; Dondero, G.; Alfonso, G. C.; de Candia, F. *Polymer* **1975**, *16*, 531.
(5) Odell, J. A.; Keller, A. *Polym. Eng. Sci.* **1977**, *17*, 544.
(6) Daniewska, I.; Picot, C. *Polym. J.* **1978**, *10*, 141.
(7) Tarasov, S. G.; Tsvankin, D. Ya.; Godovskii, Yu. K. *Polym. Sci. USSR (Engl. Transl.)* **1979**, *20*, 1728.
(8) Hashimoto, T.; Fugimura, M.; Saijo, K.; Kawai, H.; Diamant, J.; Shen, M. *Adv. Chem. Ser.* **1979**, *No. 176*, 257.
(9) Hadziioannou, G.; Mathis, A.; Skoulios, A. *Colloid Polym. Sci.* **1979**, *257*, 337, 344.
(10) Pakula, T.; Saijo, K.; Kawai, H.; Hashimoto, T. *Macromolecules* **1985**, *18*, 1294.
(11) Séguéla, R.; Prud'homme, J. *Macromolecules* **1978**, *11*, 1007.
(12) Séguéla, R.; Prud'homme, J. *Macromolecules* **1981**, *14*, 197.
(13) Oster, G.; Riley, D. P. *Acta Crystallogr.* **1952**, *5*, 272.
(14) Brown, D. S.; Fulcher, K. U.; Wetton, R. E. *J. Polym. Sci., Polym. Lett. Ed.* **1970**, *8*, 659.
(15) Lewis, P. R.; Price, C. *Polymer* **1971**, *12*, 258.
(16) Skoulios, A. *Macromolecules* **1971**, *4*, 268.
(17) Campos-Lopez, E.; McIntyre, D.; Fetters, L. J. *Macromolecules* **1973**, *6*, 415.
(18) Krigbaum, W. R.; Yazgan, S.; Tolbert, W. R. *J. Polym. Sci., Polym. Phys. Ed.* **1973**, *11*, 511.
(19) Klug, H. P.; Alexander, L. E. *X-Ray Diffraction Procedures*; Wiley-Interscience: New York, 1974; p 445.
(20) Le Meur, J.; Terrisse, J.; Schwab, C.; Goldzene, P. *J. Phys. (Paris) Colloq.* **1971**, *32*, C5a-301.
(21) Hashimoto, T.; Fujimura, M.; Kawai, H. *Macromolecules* **1980**, *13*, 1660.
(22) Richards, R. W.; Thomason, J. L. *Polymer* **1981**, *22*, 581.
(23) Bates, F. S.; Cohen, R. E.; Berney, C. V. *Macromolecules* **1982**, *15*, 589.
(24) Hoffmann, M.; Kampf, G.; Kromer, H.; Pampus, G. *Adv. Chem. Ser.* **1971**, *No. 99*, 351.
(25) Meier, D. J. *J. Appl. Polym. Sci., Appl. Polym. Symp.* **1974**, *No. 24*, 67.
(26) Guinier, A. *X-Ray Diffraction*; W. H. Freeman and Co.: San Francisco, 1963; p 323.